Electronic Supplementary Material (ESI) for Physical Chemistry Chemical Physics.

Supporting Information

Bandgap widening through doping for improving the photocatalytic oxidation ability of narrow-gap semiconductors

Yue Yang,[a] Masayuki Toyoda,[b] Akira Yamaguchi,[a] Yohei Cho,[a] An Niza El Aisnada,[a] Hideki Abe,[c] Shigenori Ueda,[d,e,f] Sayuri Okunaka,[g] Susumu Saito, [b,h,i] Min Liu,[j] Hiromasa Tokudome [k,*], Masahiro Miyauchi[a,*]

[a.] *Department of Materials Science and Engineering, School of Materials and Chemical Technology, Tokyo Institute of Technology, 2-12-1 Ookayama, Meguro, Tokyo 152-8552, Japan.*
[b.] *Department of Physics, School of Science, Tokyo Institute of Technology, 2-12-1 Ookayama, Meguro, Tokyo 152-8551, Japan.*
[c.] *Center for Green Research on Energy and Environmental Materials, National Institute for Materials Science, 1-1, Namiki, Tsukuba, Ibaraki 305-0044, Japan.*
[d.] *Synchrotron X-ray Station at SPring-8, National Institute for Materials Science, 1-1-1 Kouto, Sayo, Hyogo 679-5148, Japan.*
[e.] *Research Center for Advanced Measurement and Characterization, National Institute for Materials Science, 1-2-1 Sengen, Tsukuba, Ibaraki 305-0047, Japan.*
[f.] *Research Center for Functional Materials, National Institute for Materials Science, 1-1 Namiki, Tsukuba, Ibaraki 305-0044, Japan.*
[g.] *Global Zero Emission Research Center (GZR), National Institute of Advanced Industrial Science and Technology (AIST), 16-1 Onogawa, Tsukuba, Ibaraki, 305-8559, Japan.*
[h.] *Advanced Research Center for Quantum Physics and Nanoscience, Tokyo Institute of Technology, 2-12-1 Ookayama, Meguro-ku, Tokyo 152-8551, Japan.*
[i.] *Materials Research Center for Element Strategy, Tokyo Institute of Technology, 4259 Nagatsuta-cho, Midori-ku, Yokohama, Kanagawa 226-8503, Japan.*
[j.] *Hunan Joint International Research Center for Carbon Dioxide Resource Utilization, School of Physical and Electronics, Central South University, Changsha, Public Republic of China.*
[k.] *Research Institute, TOTO Ltd, 2-8-2 Honson, Chigasaki, Kanagawa 253-8577, Japan.*

Supporting information note

Note 1. La atom doping position

In the 12.5 at% La-$BiVO_4$, two Bi sites would be selected for La atom doping, so 15 kinds of combinations are available. The interatomic distances of these choices are listed in figure S1. The nearest interatomic distance of the Bi site is 3.76 Å, and the farthest one is 7.25 Å. Structure models with different doping pattern were calculated to discuss how La dopant distribution would influence the result. The nearest, the midst, and the farthest doping choice were selected for calculation (figure S2, S3, and S4 for their crystal structure). The calculation results are listed in table S1.

From Table S1, it can be seen that compared to the nearest and midst La doping choice, the total energy for the farthest La doping choice was 0.02 eV higher. Generally, higher energy indicates instability. However, in the current case, the energy difference is negligible as it is inside the error bar range of the calculation method[1,2]. On top of that, both the nearest La doping case and the midst doping case present the identical CB and VB position with 6.25 at% La-$BiVO_4$. We suspect that the localized La atoms would behave like the model with lower doping concentration.

In the current study, we adopted the distant La doping model for 12.5 at% La-$BiVO_4$ to discuss the effect caused by homogeneous La doping.

Note 2. IPA to acetone conversion reaction

The IPA to acetone conversion has been well investigated by previous research[3]. The chemical equation is described below

$$CH_3CHOHCH_3 + {}^1/_2\ O_2 \rightarrow CH_3(CO)CH_3 + H_2O$$

Note 3. Calculation detail of Bi to O bonding length in table S3

In $BiVO_4$, each Bi atom is surrounded by 8 O atoms. The average Bi to O distance is calculated from every Bi to its surrounding 8 O atoms' bonding length.

Note 4. Rietveld analysis of XRD pattern.

We conducted Rietveld analysis of XRD pattern through Fullprof[4] to evaluate the structure difference of pristine $BiVO_4$ and La-$BiVO_4$ obtained experimentally. The refinement starts with the scheelite monoclinic $BiVO_4$ reported from literature[5]. The Rietveld analysis result of pristine $BiVO_4$ and 10 at% La-$BiVO_4$ are shown in Figure S9 and Figure S10, respectively.

In a Rietveld analysis, the weighted profile factor (Rwp) measures the agreement between the reflection intensity calculated from a crystallographic model and those measured experimentally. And the Bragg R-factor depends on the fitting of the structure parameters rather than the profile parameters. In our Rietveld analysis, the Rwp value reached 10.1 % and 11.6 % for pristine $BiVO_4$ and 10 at% La-$BiVO_4$, respectively. Moreover, the Bragg R-factor reaches 7.33 % and 3.65 % for pristine $BiVO_4$ and 10 at% La-BiVO4, respectively, indicating a good fitting of structural

parameters. The structural parameters of the experimentally synthesized materials are listed in table S6.

Note 5. Tauc plot calculation

The bandgap of $BiVO_4$ and La-$BiVO_4$ was calculated using Tauc plots with hv as the x-axis, and $(\alpha hv)^{1/r}$ as the y axis, where h, v, and α represent the Planck constant, the frequency of light, and the Kubelka- Munk value obtained from UV-Vis spectra, respectively. The value of r is determined by the semiconductors' property: for direct bandgap semiconductors, r is 1/2, while for indirect bandgap semiconductors, r is 2. According to the previous research[6], $BiVO_4$ is a direct bandgap semiconductor, so we use r = ½ for tauc plot calculation.

Note 6. Internal quantum efficiency calculation

The absorbed photon number was calculated using the following equation:

$$N_{ads_{photon}}(mol) = \frac{1}{N_A}\int_{300\,nm}^{800\,nm}\frac{\lambda P(\lambda)SR(\lambda)}{hc}(\frac{l'}{l})d\lambda$$

In which:

- λ refers to wavelength.

-P(λ) refers to the spectral power density distribution measured by USHIO USR-45 spectroradiometer.

- S refers to the irradiation area of the photocatalyst.

- R(λ) represents the reflection ratio measured by UV-Vis spectroscopy of the material.

h, c and N_A are Planck constant, light velocity and Avogadro number, respectively.

The internal quantum yield was calculated using the following equation

$$\Phi = \frac{n_{acetone}}{N_{ads\ photon}} \times 100\%$$

In which $n_{acetone}$ is the amount of acetone molecules, $N_{ads\ photon}$ is the adsorbed photon number.

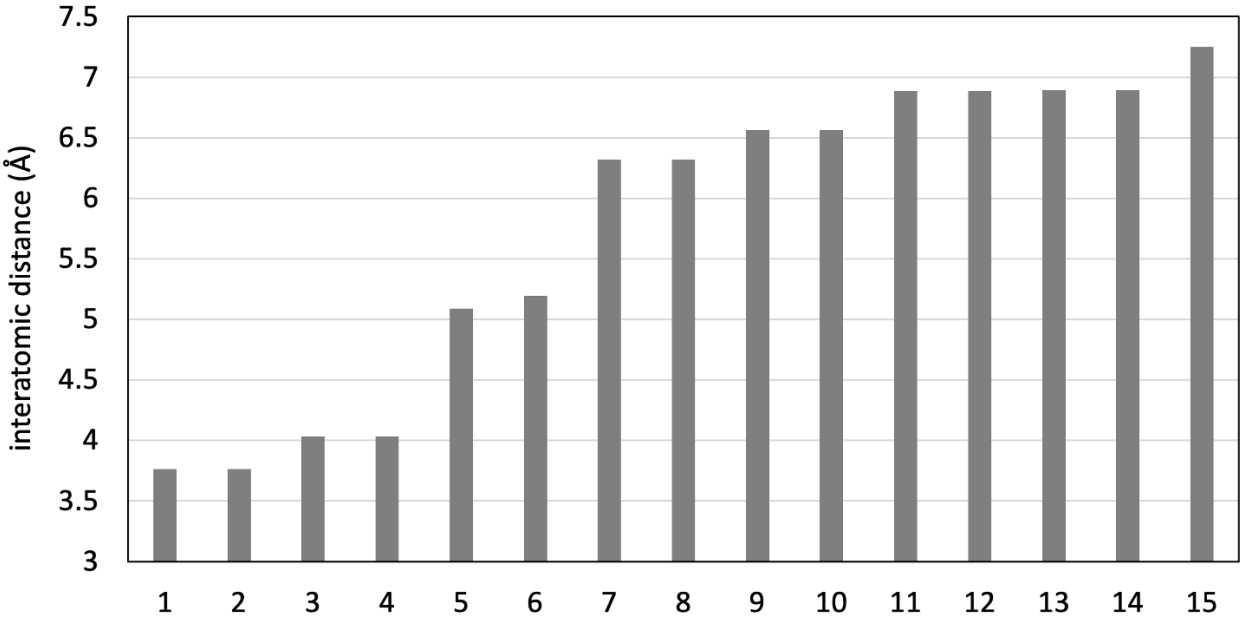

Figure S1 The interatomic distances of the two different Bi sites in $BiVO_4$ supercell.

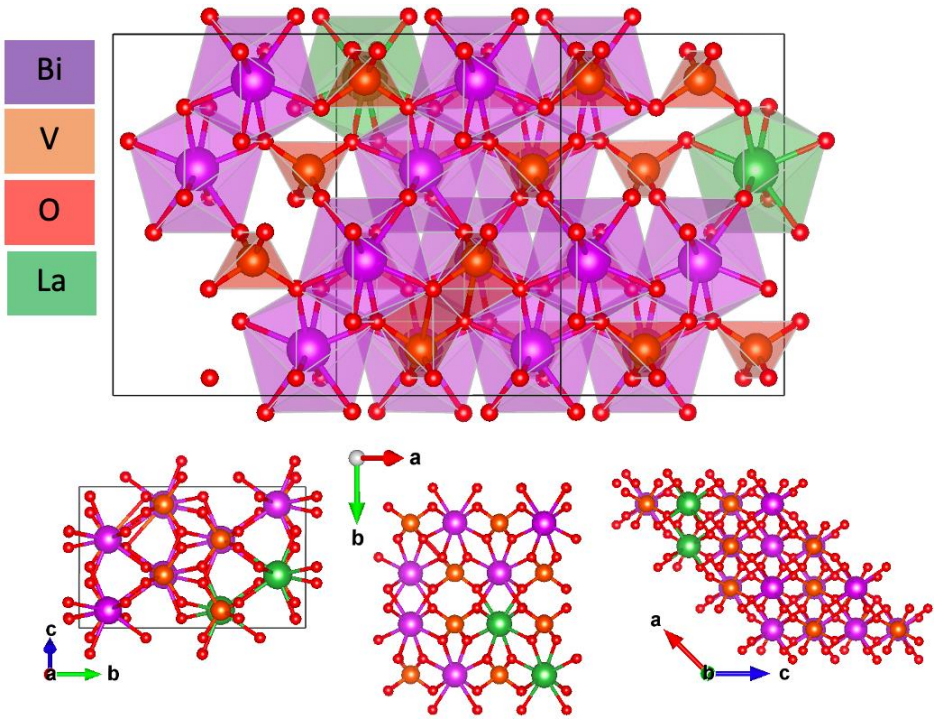

Figure S2 The structure of the 12.5 at% La-$BiVO_4$ with nearest La doping choice.

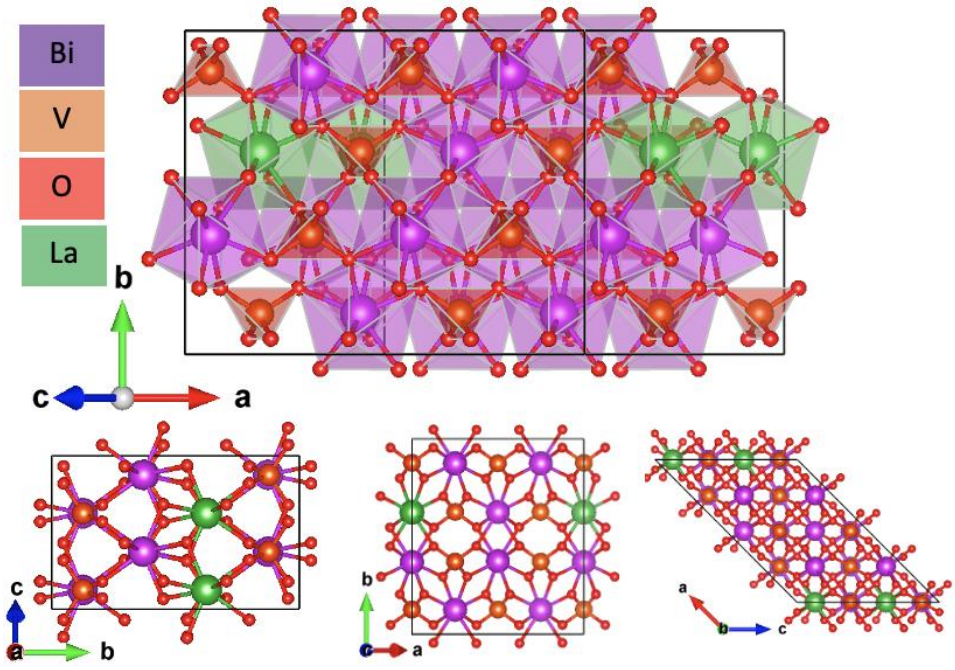

Figure S3 The structure of the 12.5 at% La-$BiVO_4$ with midst La doping choice.

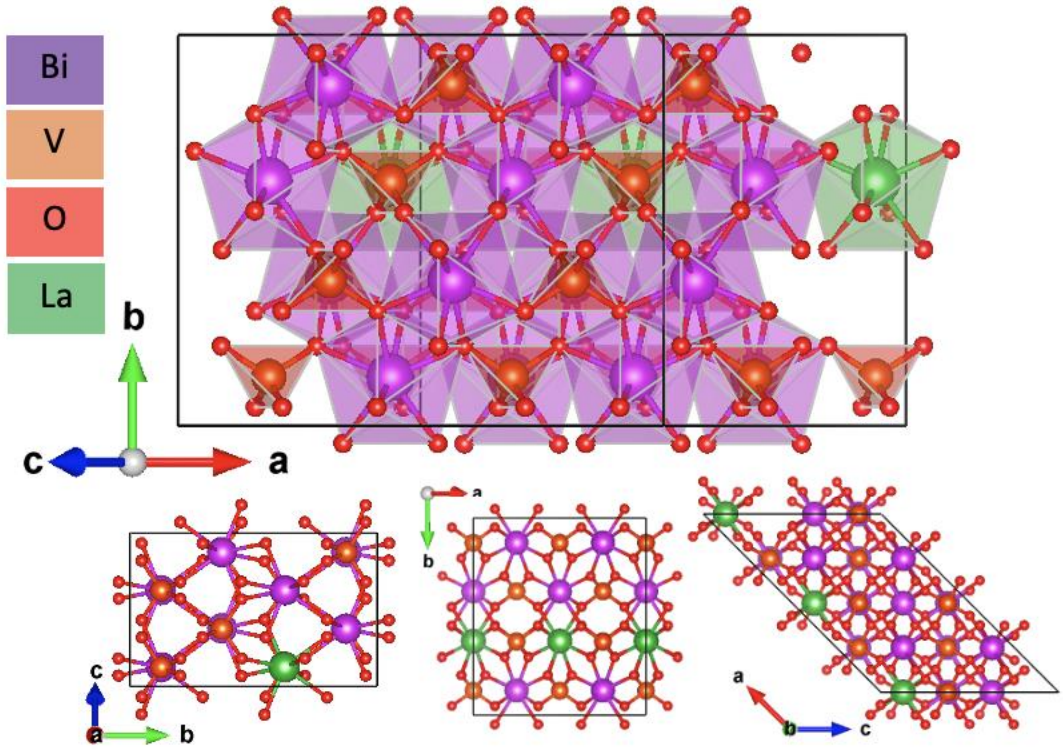

Figure S4 The structure of the 12.5 at% La-$BiVO_4$ with farthest La doping choice.

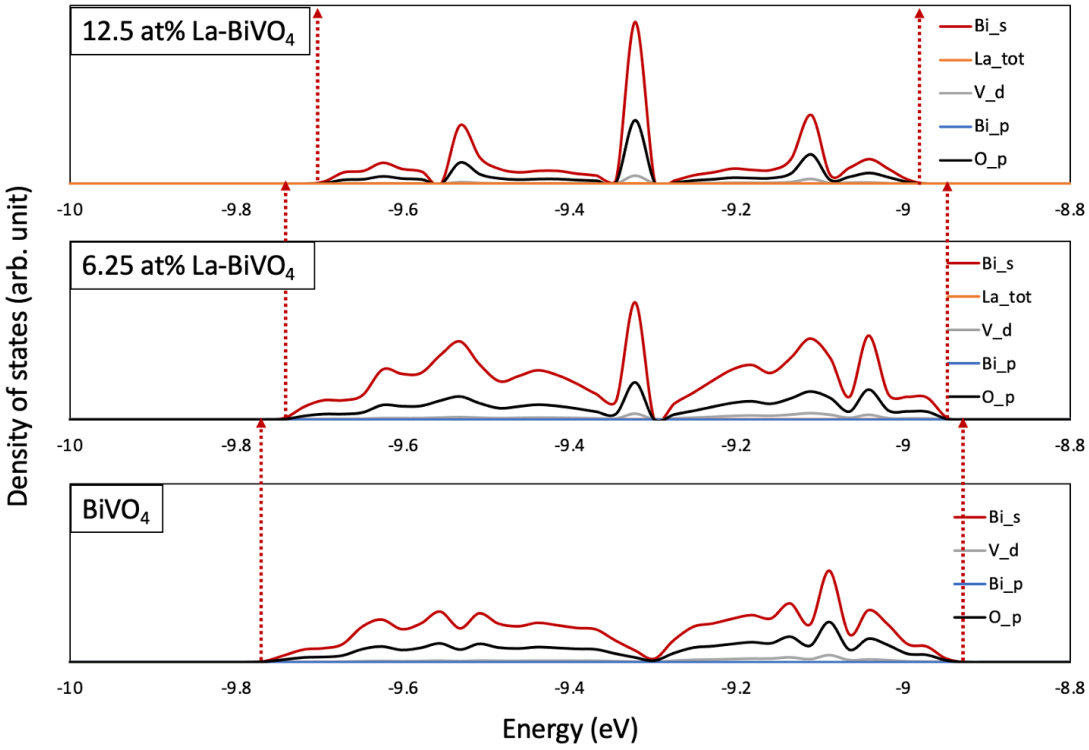

Figure S5 Enlarged DOS which mainly comprised the Bi s and O p orbitals. (The red line represents the Bi s orbitals, the black line represents the O p orbitals, V d orbital, Bi p orbital and La electronic contribution are shown by grey, blue and orange line respectively.)

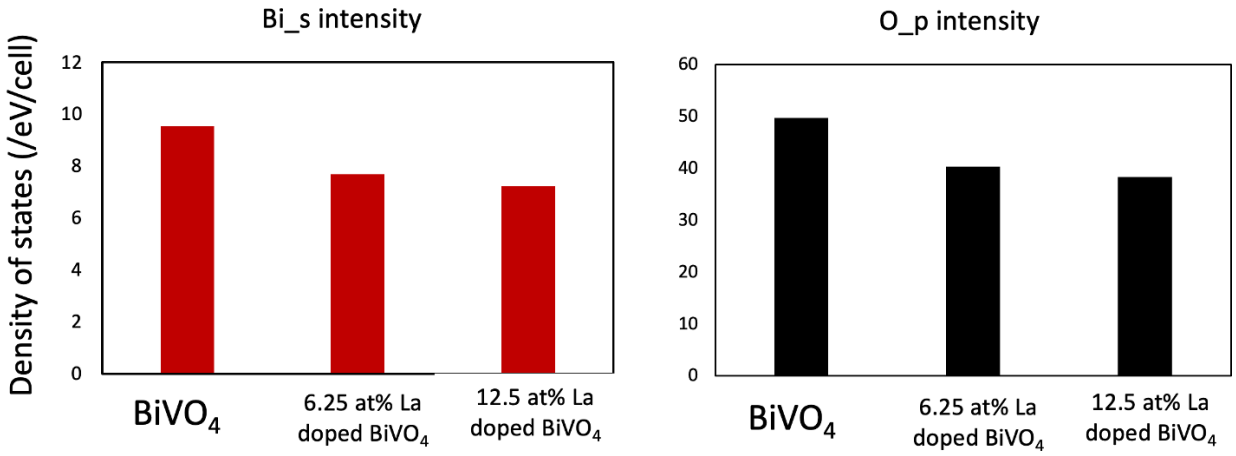

Figure S6 Intensity of Bi s and O p orbitals formed at the VB top of different structures.

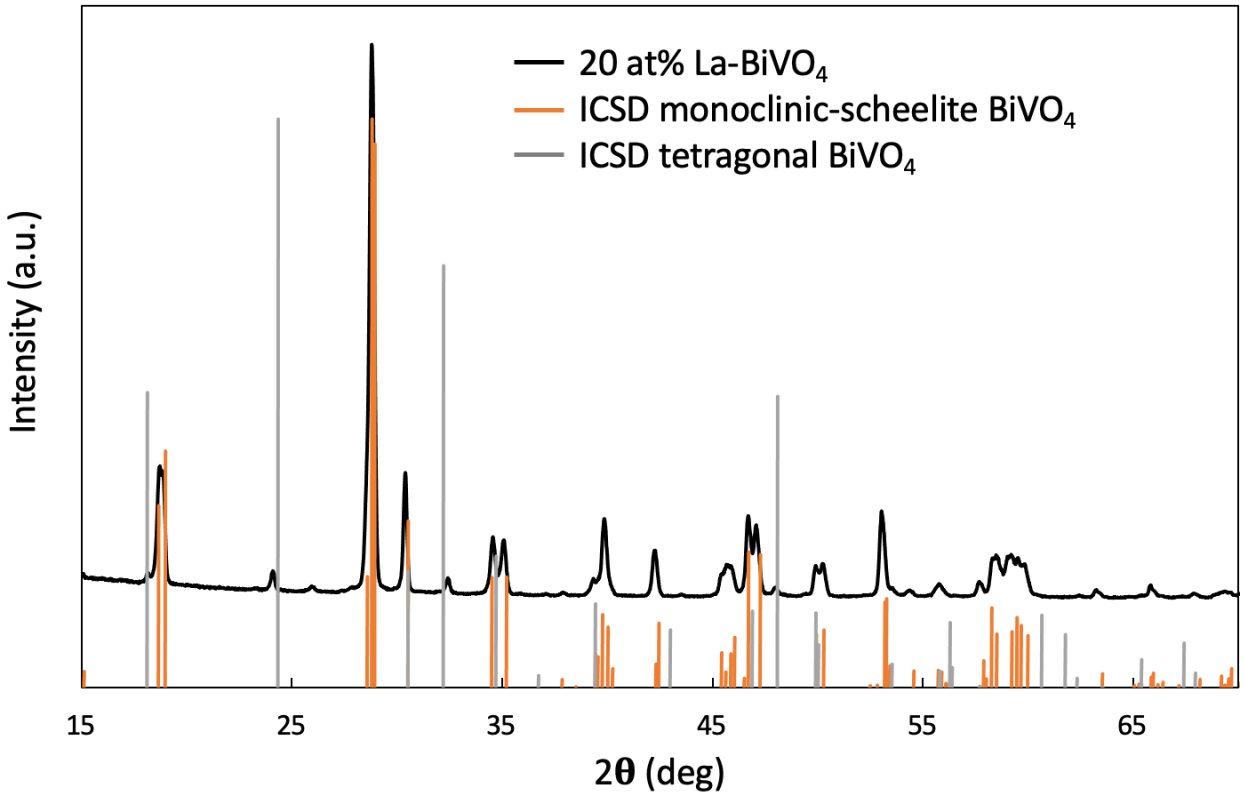

Figure S7 XRD pattern of 20 at% La-$BiVO_4$, both monoclinic and tetragonal phases exist in the material.

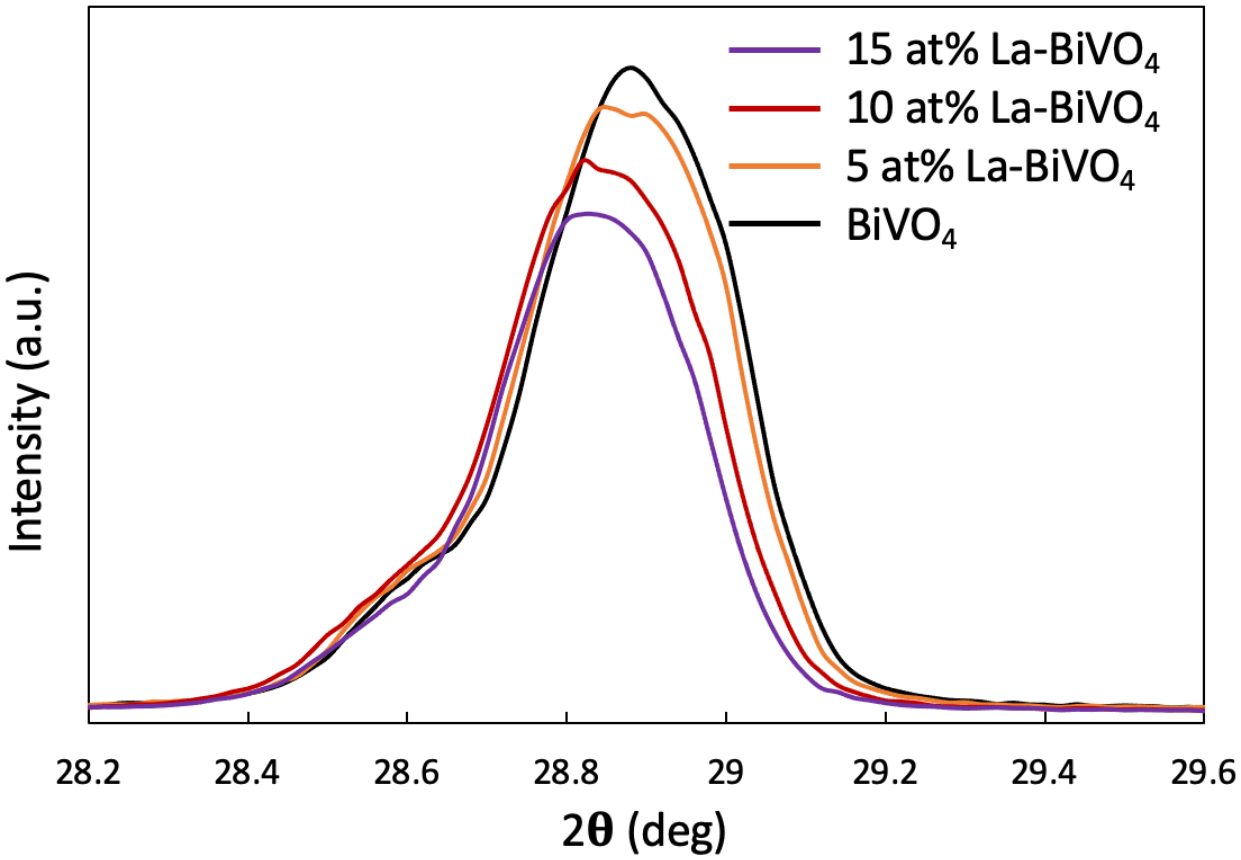

Figure S8 Comparison of XRD peak intensity of pristine and La-$BiVO_4$.

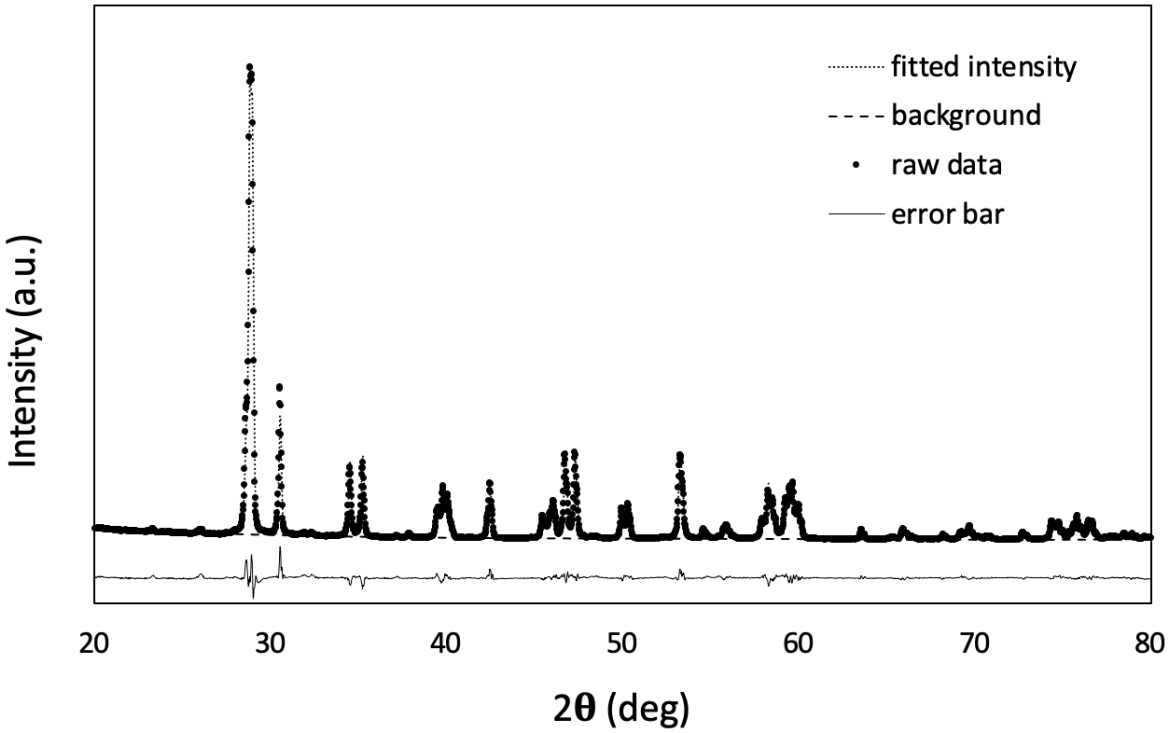

Figure S9 Rietveld analysis result of the pristine $BiVO_4$

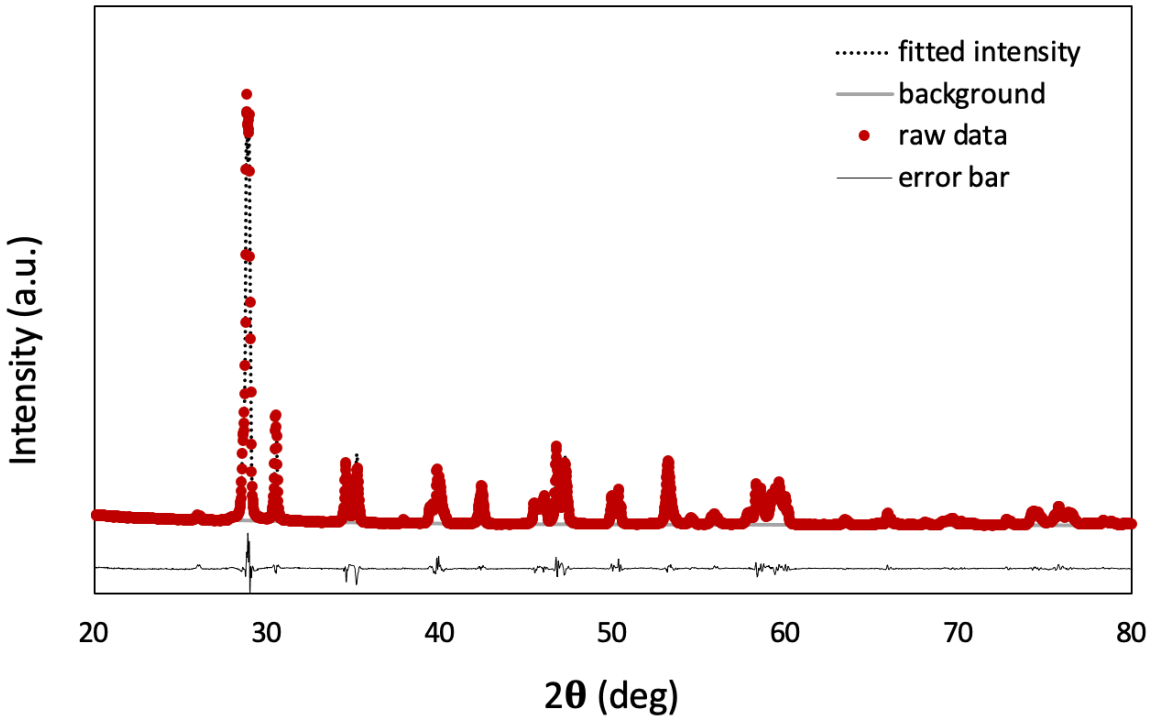

Figure S10 Rietveld analysis result of the 10 at% La-$BiVO_4$

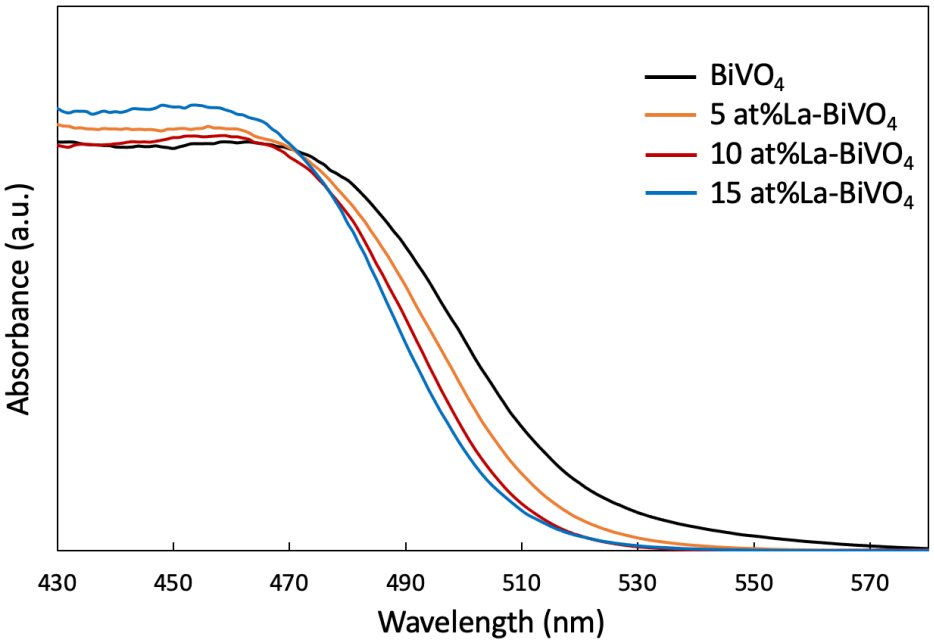

Figure S11 UV-Vis light absorption spectra of pristine $BiVO_4$ and La-$BiVO_4$.

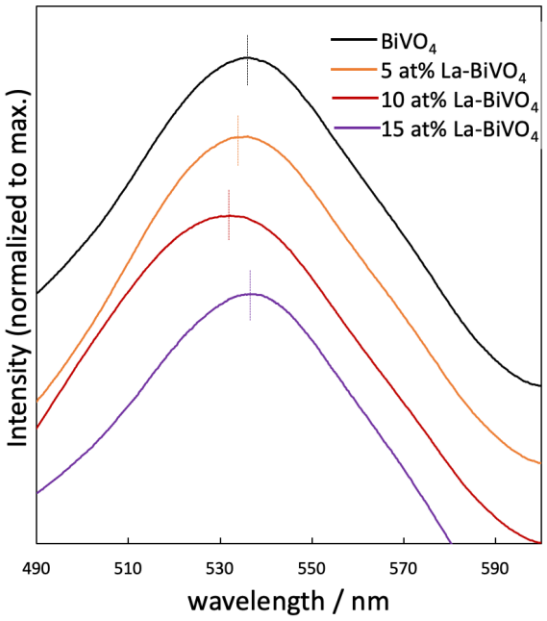

Figure S12 Photoluminescence spectra with an excitation wavelength at 355 nm for the pristine $BiVO_4$, 5 at% La-$BiVO_4$, 10 at% La-$BiVO_4$, and 15 at% La-$BiVO_4$, respectively. The peak intensity were normalized to the maximum intensity to show the gradual shift in emission peak wavelength.

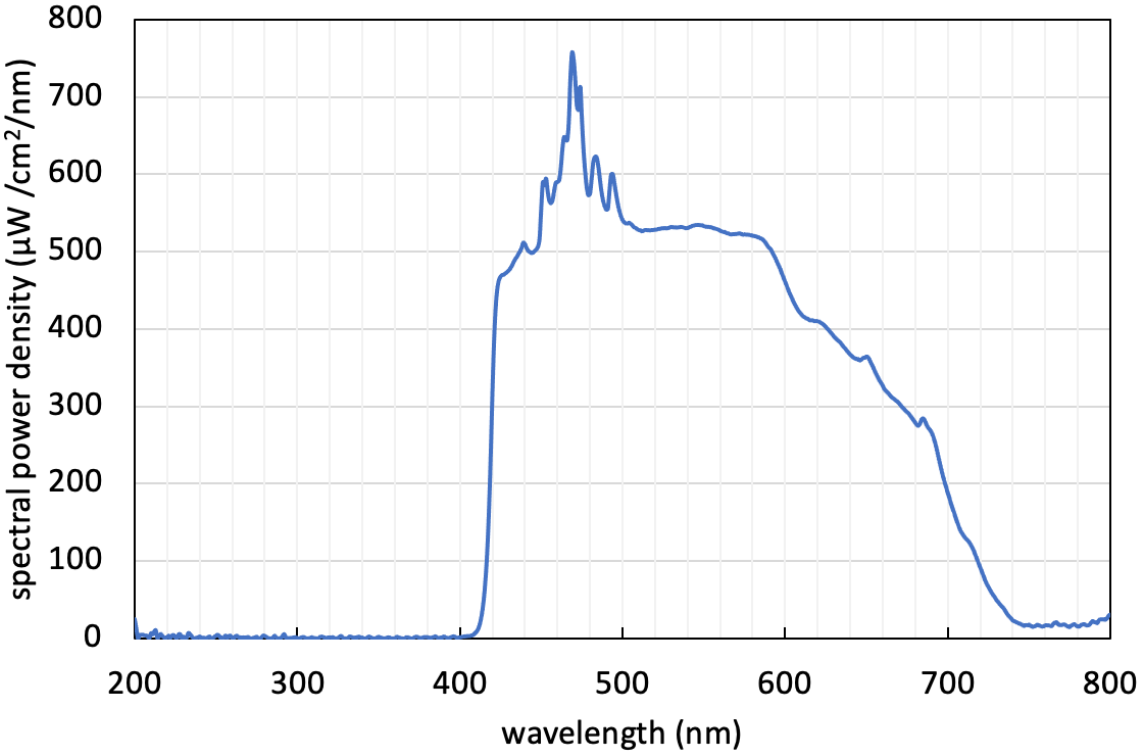

Figure S13 Spectra of xenon lamp equipped with a 422 nm cutoff filter.

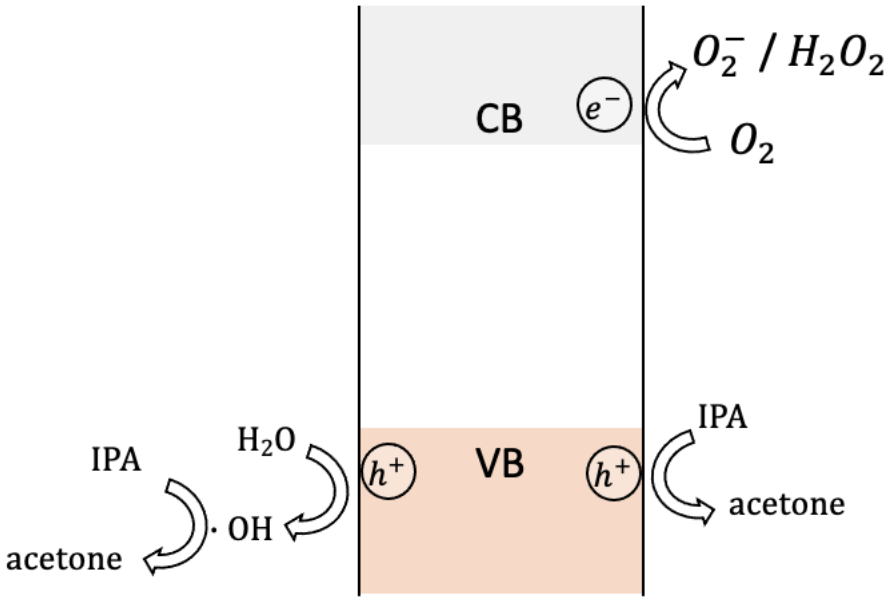

Figure S14 Schematic illustration for the photocatalytic oxidation of 2-propanol to acetone over La–$BiVO_4$

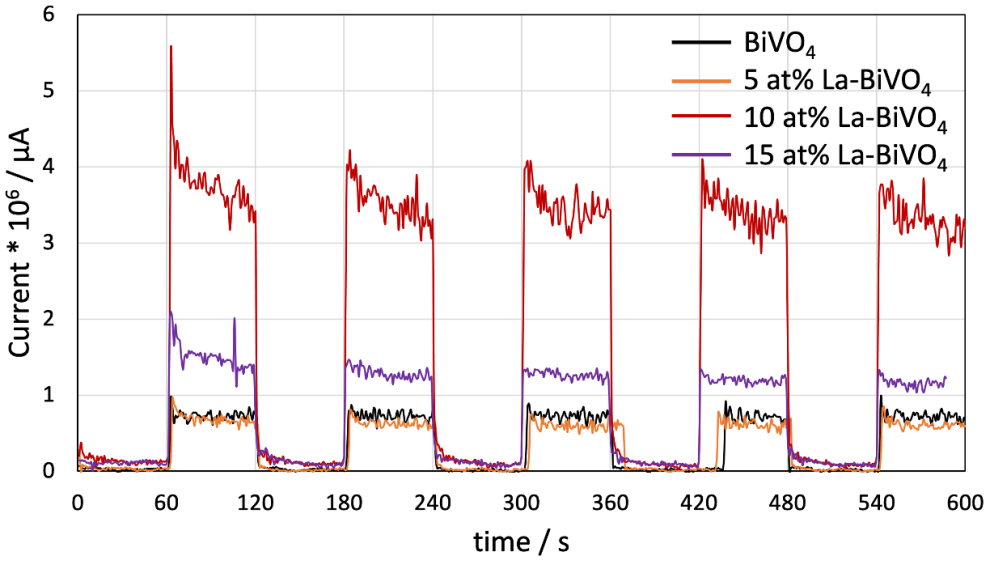

Figure S15 Photocurrent properties of $BiVO_4$ and La doped $BiVO_4$ electrodes under a Xe lamp irradiation passed through a 450 nm bandpass filter with the bias potential of 1.23 V vs RHE.

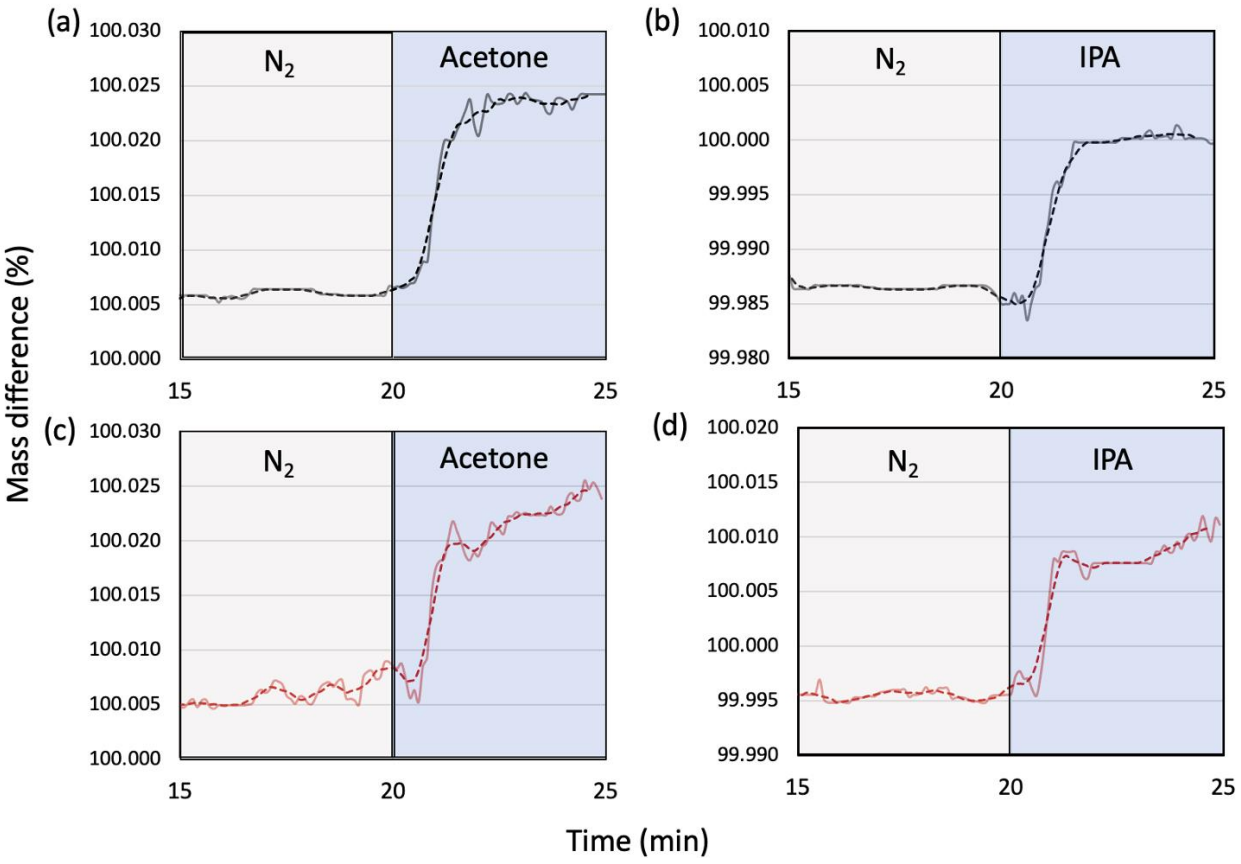

Figure S16 Gaseous acetone and IPA adsorption property over $BiVO_4$ and 10 at% La-$BiVO_4$. Figure (a) and (b) represent the acetone and IPA adsorption property over pristine $BiVO_4$, respectively. Figure (c) and (d) represent the acetone and IPA adsorption property over 10 at% La-$BiVO_4$, respectively.

We compared the gaseous acetone and IPA adsorption property through TG-DTA analysis. We kept the temperature at 25 °C during the analysis since it is the condition that we used for activity evolution.

Nitrogen was purged for the initial 20 minutes, then IPA or acetone gas was purged continuously for 5 min. The mass difference during the targeted gas purging process was recorded, as summarized in table S9.

Table S1 Calculation result of 12.5 at% La-$BiVO_4$ with different doping position choices.

Structure	interatomic distance of La (after ionic relaxation)	CB (eV)	VB (eV)	Bandgap (eV)	Total Energy (eV)
farthest La	7.31 Å	2.049	-0.075	2.124	-722.06
midst La	5.17 Å	2.049	-0.052	2.101	-722.08
nearest La	3.96 Å	2.049	-0.052	2.101	-722.08

Table S2 Structural parameters of each optimized structure obtained after ionic relaxation step.

Structure name	$BiVO_4$	6.25 at% La-$BiVO_4$	12.5 at% La-$BiVO_4$
$2 \times a$ (Å)	14.60532	14.61680	14.62336
b (Å)	11.74568	11.76554	11.78549
$2 \times c$ (Å)	10.31987	10.33069	10.33069
β (°)	134.9224	134.9494	134.8804

Table S3 Average Bi to O bonding length in different structures

Structure name	Average Bi to O bonding length (Å)
Pristine $BiVO_4$	2.471
6.25 at% La-$BiVO_4$	2.473
12.5 at% La-$BiVO_4$	2.475

Table S4 Bandwidth of the DOS shown in Figure S5.

Structure name	Bandwidth (eV)
Pristine $BiVO_4$	0.87
6.25 at% La-$BiVO_4$	0.79
12.5 at% La-$BiVO_4$	0.73

Table S5 Full width at half maximum (FWHM) of the XRD peak described in Figure S8

sample	FWHM (2theta/rad)
$BiVO_4$	0.29
5 at% La-$BiVO_4$	0.30
10 at% La-$BiVO_4$	0.32
15 at% La-$BiVO_4$	0.30

Table S6 Structural parameters of pristine $BiVO_4$ and La-$BiVO_4$ obtained from Rietveld analysis

Structure name	Pristine $BiVO_4$	10 at% La-$BiVO_4$
a	7.25155	7.25192
b	11.70300	11.72590
c	5.09299	5.10022
β	134.227	134.296
volume	309.718208	310.416126

Table S7 ICP analysis result of La-$BiVO_4$, weight ratios, and atomic ratios of La to Bi.

Structure name	element	Weight percent	Atomic percent
5 at% La-$BiVO_4$	Lanthanum	2.2 %	5.1 %
	Bismuth	61 %	95 %
10 at% La-$BiVO_4$	Lanthanum	4.6 %	10.4 %
	Bismuth	59.1 %	90 %
15 at% La-$BiVO_4$	Lanthanum	6.7 %	15.4 %
	Bismuth	55.1 %	85 %

Table S8 Binding energy of each orbital obtained from HAXPES.

Sample name	La $3d_{5/2}$	Bi $4f_{7/2}$	V $2p_{3/2}$	O 1s
$BiVO_4$		159.45 eV	517.15 eV	530.4 eV
5 at% La-$BiVO_4$	834.95 eV	159.45 eV	517.15 eV	530.4 eV
10 at% La-$BiVO_4$	834.95 eV	159.55 eV	517.25 eV	530.5 eV
15 at% La-$BiVO_4$	834.95 eV	159.55 eV	517.25 eV	530.5 eV

Table S9 Mass difference of IPA and acetone over pristine $BiVO_4$ and 10 at% La-$BiVO_4$ respectively.

Sample	Mass difference of acetone	Mass difference of IPA
$BiVO_4$	0.02 %	0.015 %
10 at% La-$BiVO_4$	0.02 %	0.015 %

Table S10 surface area of pristine $BiVO_4$ and La-$BiVO_4$

Sample	Surface area (m^2/g)
$BiVO_4$	0.6651
5 at% La-$BiVO_4$	0.4147
10 at% La-$BiVO_4$	0.3876
15 at% La-$BiVO_4$	0.7952

References in Supporting Information

(1) Lany, S. Semiconductor Thermochemistry in Density Functional Calculations. *Phys. Rev. B* **2008**, *78* (24), 245207. https://doi.org/10.1103/PhysRevB.78.245207.

(2) Zhang, Y.; Kitchaev, D. A.; Yang, J.; Chen, T.; Dacek, S. T.; Sarmiento-Pérez, R. A.; Marques, M. A. L.; Peng, H.; Ceder, G.; Perdew, J. P.; Sun, J. Efficient First-Principles Prediction of Solid Stability: Towards Chemical Accuracy. *Npj Comput. Mater.* **2018**, *4* (1), 9. https://doi.org/10.1038/s41524-018-0065-z.

(3) Arsac, F.; Bianchi, D.; Chovelon, J. M.; Ferronato, C.; Herrmann, J. M. Experimental Microkinetic Approach of the Photocatalytic Oxidation of Isopropyl Alcohol on TiO_2. Part 1. Surface Elementary Steps Involving Gaseous and Adsorbed C_3H_xO Species. *J. Phys. Chem. A* **2006**, *110* (12), 4202–4212. https://doi.org/10.1021/jp055342b.

(4) Rodríguez-Carvajal, J. Recent Advances in Magnetic Structure Determination by Neutron Powder Diffraction. *Phys. B Condens. Matter* **1993**, *192* (1–2), 55–69. https://doi.org/10.1016/0921-4526(93)90108-I.

(5) Sleight, A. W.; Chen, H. -y.; Ferretti, A.; Cox, D. E. Crystal Growth and Structure of BiVO4. *Mater. Res. Bull.* **1979**, *14* (12), 1571–1581. https://doi.org/10.1016/0025-5408(72)90227-9.

(6) Hong, S. J.; Lee, S.; Jang, J. S.; Lee, J. S. Heterojunction BiVO4/WO3 Electrodes for Enhanced Photoactivity of Water Oxidation. *Energy Environ. Sci.* **2011**, *4* (5), 1781. https://doi.org/10.1039/c0ee00743a.